Acta Mechanica 135, 153 – 167 (1999)

ACTA MECHANICA

Numerical study of disk driven rotating MHD flow of a liquid metal in a cylindrical enclosure

R. Bessaih, Constantine, Algeria, **Ph. Marty**, Grenoble, France, and **M. Kadja,** Constantine, Algeria

(Received March 9, 1998; revised April 28, 1998)

Summary. A numerical study of the steady laminar MHD flow driven by a rotating disk at the top of a cylinder filled with a liquid metal is presented. The governing equations in cylindrical coordinates are solved by a finite volume method. The effect of an axial magnetic field on the flow is investigated for an aspect ratio H/R equal to 1. The magnetic Reynolds number is assumed to be small whereas the interaction parameter, N, is large compared to unity. This allows to derive asymptotic results for the flow solution which are found in good agreement with the numerical calculations. The effect of the top, bottom and vertical walls conductivity on the flow is studied. Various combinations of these conductivities are considered. The results obtained showed that one can control the primary flow through a good choice of the electrical conductivity of both the disk and cylinder walls.

Notation

B	Magnetic field
H	Height of the cylinder
Ha	Hartmann number
jz	Axial electric current
N	Interaction parameter
P	Dimensionless pressure
R	Radius of the cylinder
Re	Reynolds number
R_m	Magnetic Reynolds number
r	Dimensionless radius
V_r	Dimensionless radial velocity
V_z	Dimensionless axial velocity
V_θ	Dimensionless azimuthal velocity
Z	Dimensionless height

Greek symbols

ϱ	Density of the fluid
υ	Kinematic viscosity
μ	Dynamic viscosity
σ	Electrical conductivity
Ω	Angular velocity
φ	Dimensionless electric potential
δ	Thickness of the Ekman layer
Δ	Laplacian operator
Δr	Increment of the grid in the radial direction
ΔZ	Increment of the grid in the axial direction

1 Introduction

The flow created by a rotating disk inside a stationary enclosure is a particular case of confined swirling flows. It is important in many areas of engineering such as rotational viscosimeters, centrifugal machinery, pumping of liquid metals at high melting point, crystal growth from molten silicon in Czochralski Crystal pullers, etc. The state-of-the-art in this field has been summarized by Granger [1] and recently by Tsitverblit and Kit [2].

Concerning the particular case of a disk driven flow in a cylindrical enclosure, literature mainly focusses on small aspect ratios ($H/R \ll 1$) (Schultz-Grunow [3], Daily and Nece [4], etc.), this configuration being more representative of the structure of many hydraulic machines (turbines, centrifugal pumps, etc.). The model of Schultz-Grunow, conceived for a geometry having a small aspect ratio, predicts that the fluid situated between the rotating disk and the stationary cover is in solid rotation. For a geometry having an aspect ratio of 1, such as the one considered in this work, the influence of the lateral walls on the flow can no longer be neglected, as was done in the study of Schultz-Grunow.

The only theoretical approaches of the flow when $H/R \approx O(1)$ are those of Grohne [5] and Thomlan and Hudson [6]. Both studies are concerned with cases where Re is asymptotically large.

The numerical simulations are numerous but are mainly restricted to Reynolds numbers comprised between 10^2 and 10^3 (see, for example, Bertela and Gori [7], Lang et al. [8], Tsitverblit and Kit [2]). Only the computations of Lang et al. have treated the case of a higher Reynolds number (10^5).

Experimental studies of this flow are few and limited either to the measurement of profiles of the azimuthal velocity component (for example Alonso [9] for $\mathrm{Re} \cong O(10^4)$) or to the visualization of the recirculating secondary flow (Escudier [10] for $\mathrm{Re} \leq 3.10^3$) and to some measurements of the velocity field (Ronnenberg [11] for $\mathrm{Re} = 1\,580$, $H/R = 1.59$).

The corresponding MHD problem has almost never been considered. One paper nevertheless [12] describes the asymptotic flow solution in a Czochralski crystal puller with an axial magnetic field of high intensity.

The present work addresses the effect of a strong magnetic field on the flow structure. The situation can be encountered in the pumping of high melting point metals such as Lithium-Lead alloys used in the cooling of future fusion reactors. As a matter of fact, creating a liquid metal flow in a closed vessel by rotating one end wall is an easy solution to study the effect of a magnetic field on the kinetics of reactions occurring at the interface between the walls and the liquid metal. This geometry has been recently proposed by Barbier et al. [13] as a small scale laboratory experiment which could provide useful informations on the effect of a strong magnetic field on the corrosion rate of stainless steels by liquid lithium-lead Pb-17Li alloys. In the present work, the effect of the electrical conductivity of the walls on the flow solution will also be studied.

2 Problem formulation

2.1 Governing equations

The geometry of the flow and the coordinate system used are shown in Fig. 1. A liquid metal with a density ϱ, a kinematic viscosity υ and an electrical conductivity σ fills a cylinder of radius R and height H submitted to an axial magnetic field B. The top end wall rotates with

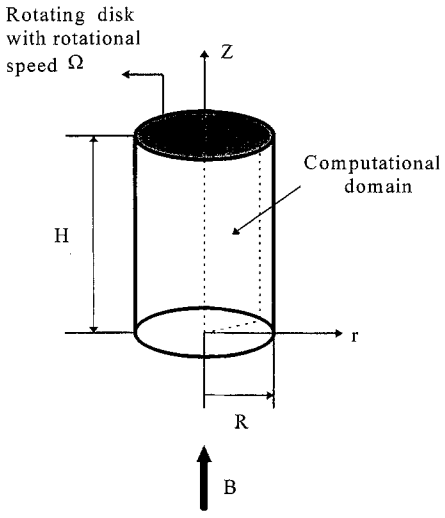

Fig. 1. Geometry of the flow

an angular velocity Ω. Using R, ΩR, $\varrho\Omega^2R^2$ and $\sigma\Omega RB$ as typical scales for the lengths, velocities, pressure and electrical current densities, respectively, the axisymmetric and dimensionless continuity and Navier Stokes equations in cylindrical coordinates become:

$$\frac{1}{r}\frac{\partial}{\partial r}(rV_r)+\frac{\partial V_Z}{\partial Z}=0\,, \tag{1}$$

$$V_r\frac{\partial V_r}{\partial r}+V_Z\frac{\partial V_r}{\partial Z}-\frac{{V_\theta}^2}{r}=-\frac{\partial P}{\partial r}+\frac{1}{\mathrm{Re}}\left(\Delta V_r-\frac{V_r}{r^2}\right)-NV_r\,, \tag{2}$$

$$V_r\frac{\partial V_\theta}{\partial r}+V_Z\frac{\partial V_\theta}{\partial Z}+\frac{V_rV_\theta}{r}=\frac{1}{\mathrm{Re}}\left(\Delta V_\theta-\frac{V_\theta}{r^2}\right)+N\left(\frac{\partial\varphi}{\partial r}-V_\theta\right), \tag{3}$$

$$V_r\frac{\partial V_Z}{\partial r}+V_Z\frac{\partial V_Z}{\partial Z}=-\frac{\partial P}{\partial Z}+\frac{1}{\mathrm{Re}}(\Delta V_Z)\,, \tag{4}$$

where φ is the electrical potential which is scaled by ΩR^2B and satisfies a Poisson equation:

$$\Delta\varphi=\frac{V_\theta}{r}+\frac{\partial V_\theta}{\partial r}\,. \tag{5}$$

In Eqs. (1)–(4), N is the interaction parameter, the ratio of the electromagnetic forces to inertia forces:

$$N=\frac{\sigma B^2}{\varrho\Omega}\,, \tag{6}$$

Re is the Reynolds number defined by:

$$\mathrm{Re}=\frac{\Omega R^2}{\upsilon}\,. \tag{7}$$

These two dimensionless numbers depend on the speed of rotation ΩR. The variables r and Z designate the dimensionless radius and height, respectively. The lateral wall is therefore situated at $r=1$, bottom wall at $Z=0$ and the rotating disk at $Z=H/R$.

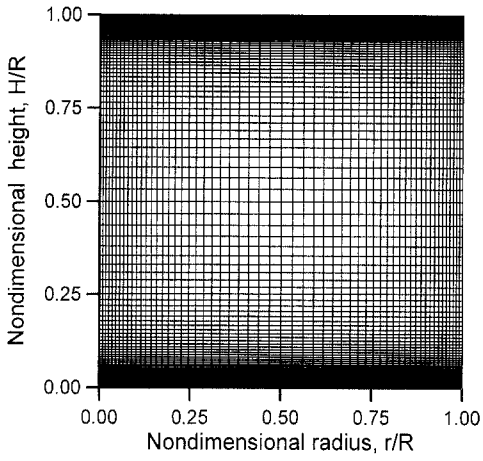

Fig. 2. Grid used in the computations

The above equations are only valid for the case of a constant magnetic field which remains unaffected by the flow. This approximation is valid as long as the magnetic Reynolds number R_m defined by

$$R_m = \mu_0 \sigma \Omega R^2 \tag{8}$$

is small, a condition which is always verified in small scale laboratory experiments. As an example, a liquid metal having an electrical conductivity $\sigma = 2.10^6\ \Omega^{-1}\,\mathrm{m}^{-1}$ in a cylinder of radius $R = 5$ cm with a disk rotating at 1 Hz provides a value of R_m equal to 0.04.

2.2 Numerical procedure

Equations (1) to (5) have been solved by using a finite volume method coupled to a pressure correction equation based on the SIMPLER Algorithm [14]. The solution in the meridional plane $r-Z$ was obtained by solving Eqs. (1), (2) and (4) for P, V_r and V_Z respectively. This is then used to obtain V_θ from Eq. (3). The φ field was subsequently computed from (5) using the values of V_θ in the meridional plane.

The increments Δr and ΔZ of the grid used (Fig. 2) are not regular. The refinement was done near the walls where the strong velocity gradients exist, thus requiring a larger number of nodes in order to reduce numerical errors. The grid used has 60×140 nodes and was chosen after performing grid independency tests.

3 Results

3.1 Solution in the absence of a magnetic field ($N = 0$)

In the absence of the magnetic field, only Eqs. (1)–(4) need to be solved with $N = 0$ imposed. The boundary conditions for each of the three velocity components are:

$$V_r(r=0) = V_r(r=1) = V_r(Z=0) = V_r(Z=H/R) = 0\,, \tag{9}$$

$$V_\theta(r=0) = V_\theta(r=1) = V_\theta(Z=0) = 0\,; \qquad V_\theta(Z=H/R) = r\,, \tag{10}$$

$$V_Z(r=1) = V_Z(Z=0) = V_Z(Z=H/R) = 0\,; \qquad \frac{\partial V_Z}{\partial r}(r=0) = 0\,. \tag{11}$$

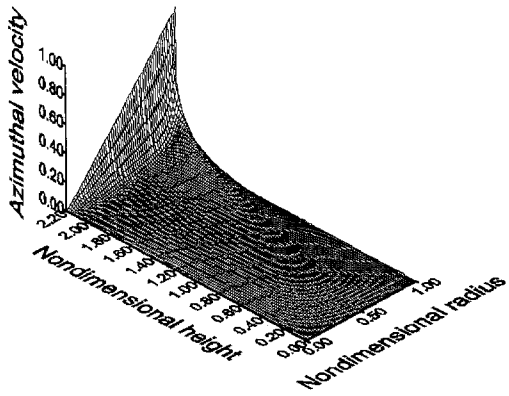

Fig. 3. Azimuthal velocity distribution for Re = 1000, $H/R = 2.2$ and $N = 0$

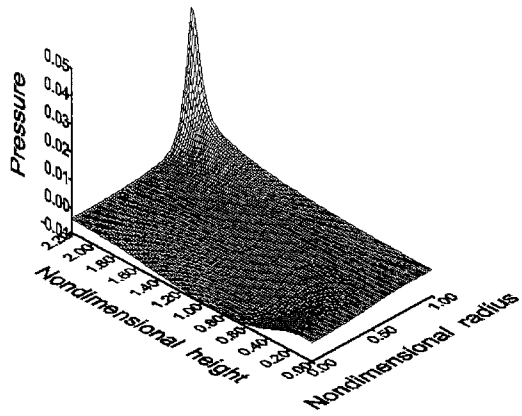

Fig. 4. Pressure field for Re = 1000, $H/R = 2.2$ and $N = 0$

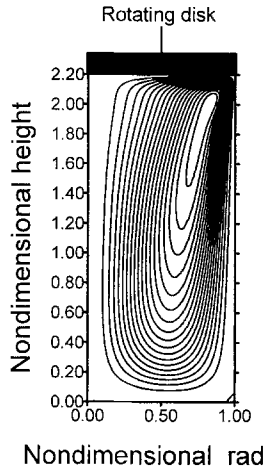

Fig. 5. Streamlines pattern for Re = 1000, $H/R = 2.2$ and $N = 0$

They express the no slip condition of the fluid at the walls, and the symmetry of the solution with respect to the axis in $r = 0$.

The results corresponding to $H/R = 2.2$ and Re = 1 000 are presented in Figs. 3–7. The primary flow is represented using the azimuthal component of the velocity V_θ, whereas the secondary flow is represented via the pressure field, the streamfunction contours and the meridional components of velocity V_r and V_Z.

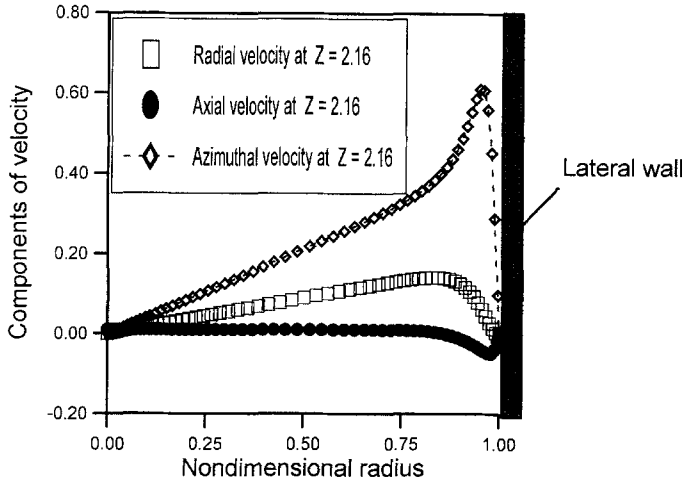

Fig. 6. Radial distribution of the radial, axial and azimuthal velocities below the rotating disk (Re = 1000, $H/R = 2.2$ and $N = 0$)

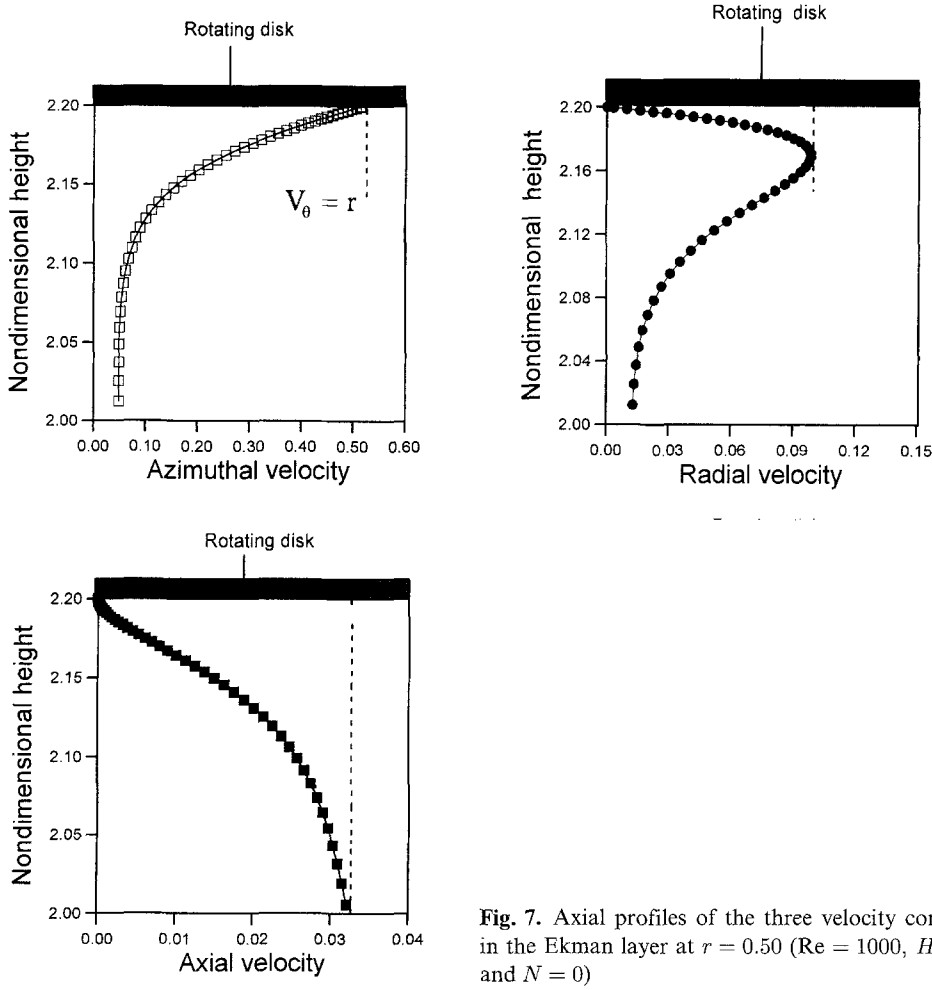

Fig. 7. Axial profiles of the three velocity components in the Ekman layer at $r = 0.50$ (Re = 1000, $H/R = 2.2$ and $N = 0$)

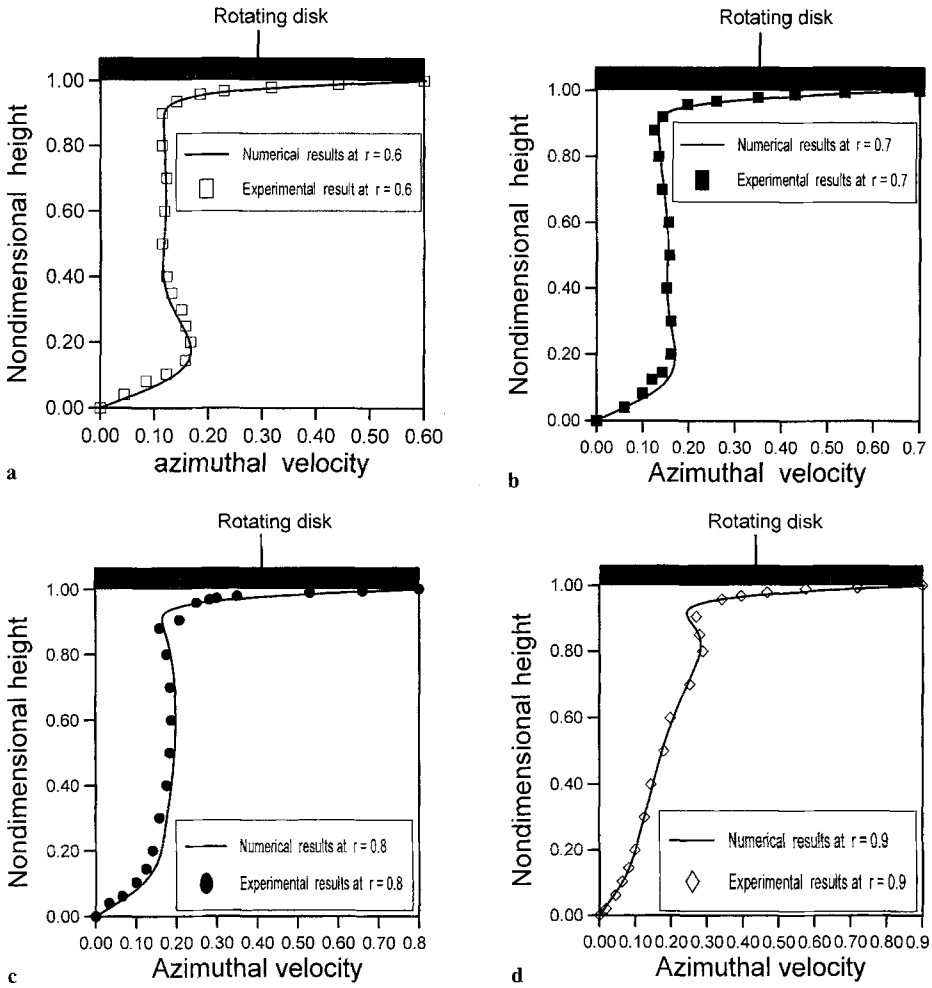

Fig. 8. Distribution of azimuthal velocity for various r positions: Comparison with experimental data [15] for Re = 1800 and $H/R = 1$

As shown from the results, an Ekman layer takes place under the rotating disk where the azimuthal velocity, V_θ, is higher than everywhere else in the cavity. From Fig. 4 representing an elevation view of the pressure field, one can notice a region of high pressure created at the point ($r = 1$, $Z = H/R$). This high pressure evacuates the fluid in the remaining parts of the enclosure, where the pressure is weaker, by pumping the liquid under the disk, a phenomenon known as Ekman pumping.

The secondary flow pattern is show in Fig. 5. The fluid rotates around a point situated near the upper right edge where the rotating disk meets the stationary side wall. The radial and vertical velocity component distributions along $r = 0.50$ are shown in Figs. 7b and 7c. The radial outflow is quite strong near the top disk, giving an intensified boundary layer under the disk. There is also a boundary layer inflow on the bottom of the enclosure.

Because of the absence of literature on experimental values of V_r, V_θ and V_Z in the Ekman layer under the disk, our numerical results can at least be compared to order of magnitude obtained from an asymptotic analysis. The leading idea of this analysis consists in writing that the outward flux of angular momentum which will flow out of the Ekman layer near the region ($r = 1$, $Z = H/R$) has its origin in the viscous friction forces exerted by the disk on the

layer between $r = 0$ and $r = 1$. This leads to the wellknown result that, in the Ekman layer which has a thickness $\delta = O(\mathrm{Re}^{-1/2})$, the radial velocity, V_r, is of the same order of magnitude as V_θ, i.e. $V_\theta = O(1)$ with our scaling quantities. An order of magnitude of the axial velocity in this layer is readily obtained from continuity:

$$V_Z = \frac{1}{\sqrt{\mathrm{Re}}}.$$

In Fig. 7 where Re = 1 000, one shows that the radial velocity V_r has a maximum value equal to 0.1, i.e. only 5 times less than V_θ which has a maximum value of 0.5 at this radius. The vertical velocity V_Z is shown in Fig. 7 c. Its value at the layer exit is 0.03, what compares fairly well with $\mathrm{Re}^{-1/2}$. Finally, the role of the boundary layer along the vertical wall in $r = 1$ can be observed in Fig. 6 where strong velocity gradients can be seen. Their origin stems from the fact that this vertical layer has to consume the flux of angular momentum delivered by the Ekman layer below the rotating disk.

In order to add further confidence to the validity of the computations, another calculation was made for a cylinder with an aspect ratio $H/R = 1.0$ where the fluid rotates at a Reynolds number of 1 800. This case has been experimentally investigated by Michelsen [15] using an LDA technique to determine velocity distributions. Figure 8 shows the azimuthal velocity component distribution along lines of constant radius. The computed values can be seen to be in excellent agreement with measurements over the whole flow field at the exception of the region near the bottom of the enclosure where slight deviations may be found. This can be circumvented by further refinement of the grid near this boundary.

3.2 Solution in the presence of a strong axial magnetic field ($N \gg 1$)

As discussed above, one of the aims of this paper is to provide informations for the study of liquid metal flows in fusion reactor technology. This type of flows is characterized by high values of the interaction parameter, N. Still considering a future Pb17-Li lithium-lead experiment where $\varrho = 10^4\,\mathrm{kg\,m^{-3}}$ and $\upsilon = 2.10^7\,\mathrm{m^2\,S^{-1}}$ with $R = 5$ cm and a disk rotating at 1 Hz, a magnetic field $B = 1$ Tesla gives $N = 31$. Inertial terms can then be simplified in Eqs. (2) to (4). This simplification yields the following modified set of momentum equations:

$$-\frac{\partial P}{\partial r} + \frac{1}{\mathrm{Re}}\left(\Delta V_r - \frac{V_r}{r^2}\right) - NV_r = 0, \tag{12}$$

$$\Delta V_\theta - \frac{V_\theta}{r^2} = \mathrm{Ha}^2\left(V_\theta - \frac{\partial \varphi}{\partial r}\right), \tag{13}$$

$$-\frac{\partial P}{\partial Z} + \frac{1}{\mathrm{Re}}\Delta V_Z = 0, \tag{14}$$

where the Hartmann number Ha is defined by

$$\mathrm{Ha} = B/R\sqrt{\frac{\sigma}{\mu}}$$

and represents the ratio of the electromagnetic forces to the viscous forces. It is related to the Reynolds number and interaction parameter by the expression

$$N = \frac{\mathrm{Ha}^2}{\mathrm{Re}}$$

and is much greater than unity.

Equation (13) for the azimuthal flow is decoupled in this case from those of the other two velocity components. It is therefore possible to solve the coupled equations for V_θ and φ (Eqs. (13) and (5)), then to use the results to obtain a solution for the meridional recirculating flow from Eqs. (1), (11) and (14).

The two particular cases of electrically insulating or perfectly conducting walls are treated first before considering intermediate situations. The calculations were performed for the following values of the Hartmann number and of the interaction parameter:

$\mathrm{Ha} = 100,$

$N = 100.$

3.2.1 Electrically insulating walls

The fluid is therefore surrounded by a totally insulating medium and the electric current lines must close within the fluid (Fig. 9 c). The flow is characterized by two distinct regions:

- the core region where the velocity gradients are weak and produce negligible viscous forces.
- the Hartmann layers situated under the rotating disk and on the bottom wall of the cylinder, in which the electric current lines becomes very close to each other and where azimuthal equilibrium is ensured via an equilibrium between the viscous forces and the electromagnetic forces.

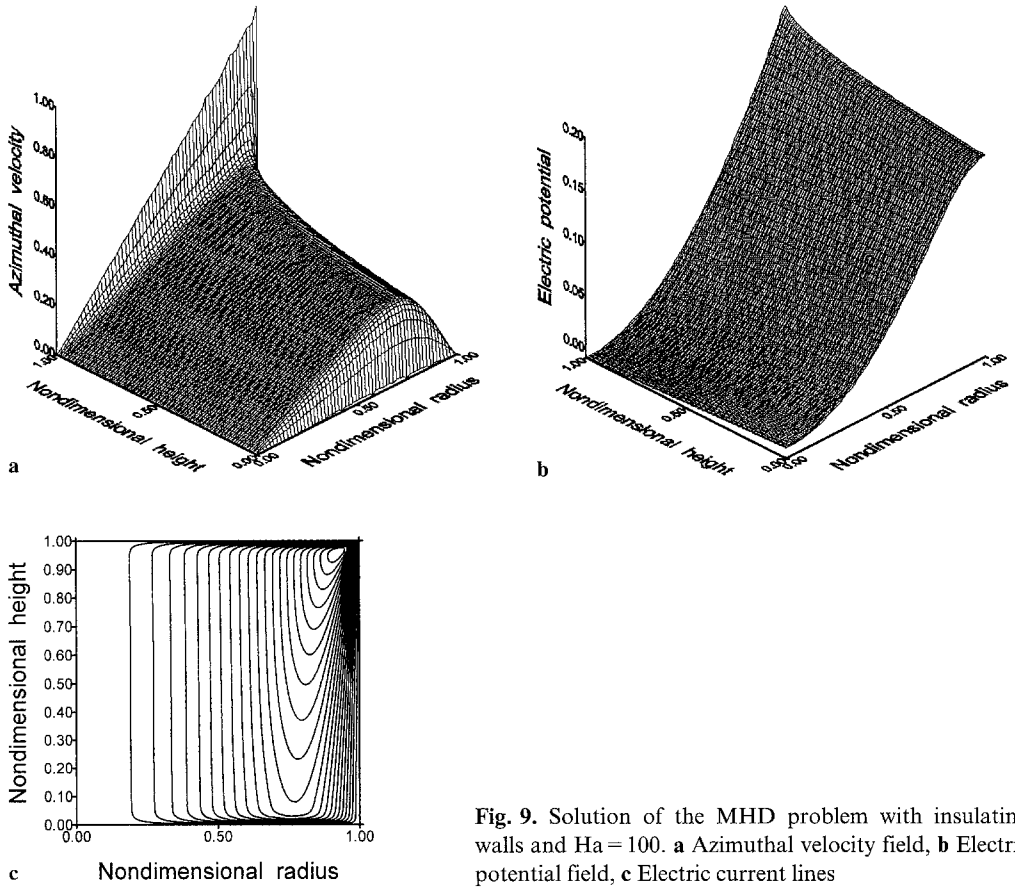

Fig. 9. Solution of the MHD problem with insulating walls and Ha = 100. **a** Azimuthal velocity field, **b** Electric potential field, **c** Electric current lines

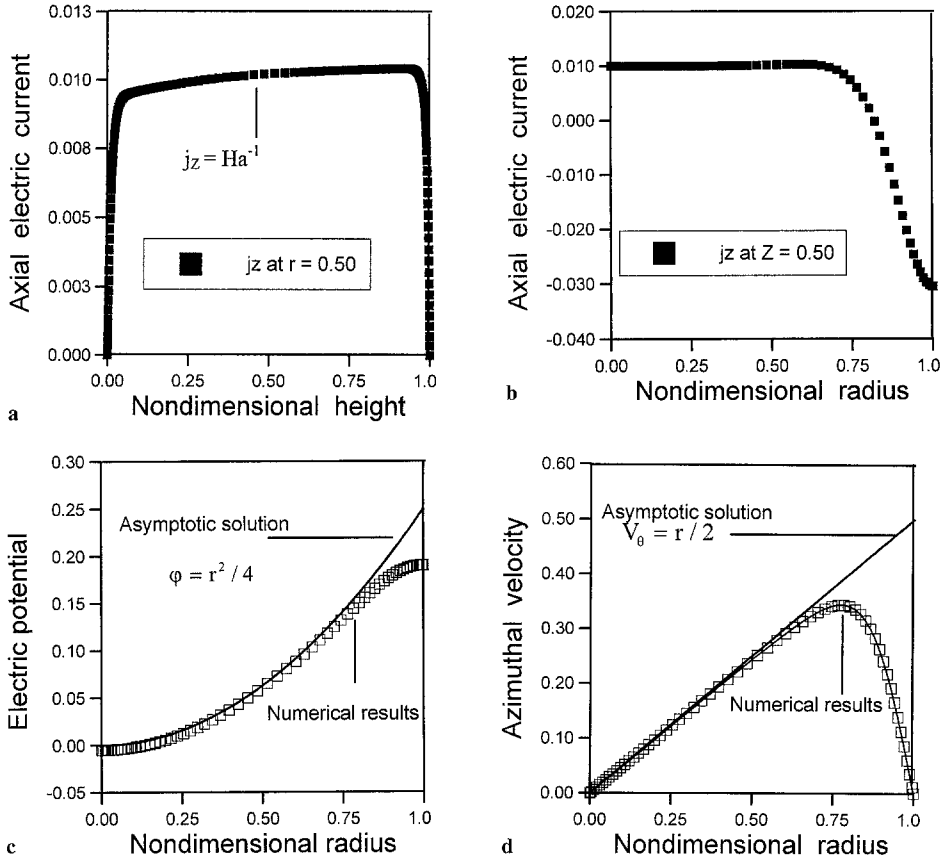

Fig. 10. Insulating walls. Electric current, potential and azimuthal velocity distributions, for $H/R = 1$ and Ha = 100. **a** Distribution of the axial electric current at $r = 0.50$, **b** Distribution of the axial electric current at $Z = 0.50$, **c** Distribution of the electric potential at $Z = 0.50$: comparison with asymptotic solution, **d** Distribution of the azimuthal velocity component at $Z = 0.50$: comparison with asymptotic solution

The boundary conditions used for the electrical potential are:

$$\frac{\partial \varphi}{\partial Z}(Z=0) = \frac{\partial \varphi}{\partial Z}(Z=1) = \frac{\partial \varphi}{\partial r}(r=0) = \frac{\partial \varphi}{\partial r}(r=1) = 0$$

and express the cancelling of the normal component of the electric current at the boundary between the fluid and the insulating walls. The boundary conditions for the velocities remain the same as those given in Eqs. (9)–(11).

Figure 9 shows the azimuthal velocity field, the electrical potential field and isocurrent lines, and Fig. 10 gives profiles at $r = 0.50$ or $Z = H/R = 0.50$ of the electric current, the electric potential and the azimuthal velocity. The results shown in Figs. 10c and 10d are in good agreement with the asymptotic solution:

$$V_\theta = \frac{r}{2},$$

$$\varphi = \frac{r^4}{4} - \frac{Z}{\mathrm{Ha}},$$

which satisfies the azimuthal equilibrium in the core of the flow. The rigid body rotating core is crossed by an axial electric current $j_z = O(\mathrm{Ha}^{-1})$ which also circulates through the top and bottom Hartmann layers of thickness Ha^{-1} as it is shown in Fig. 9 c. The total electric current in these Hartmann layers is then of order of unity. The global contribution of the electromagnetic forces in the azimuthal direction is zero, what requires that the core will be in azimuthal equilibrium between the viscous driving stress from the disk at the top and the viscous braking at the bottom wall. This is another possibility to understand why the core rotates at a velocity which is an exact average between that of the two end walls.

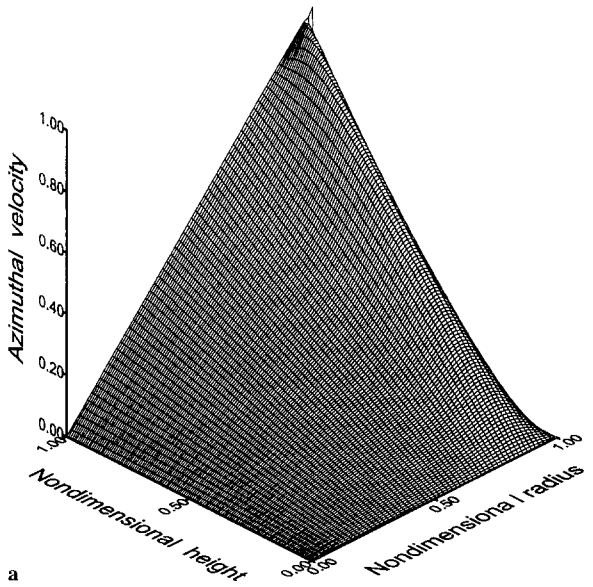

a

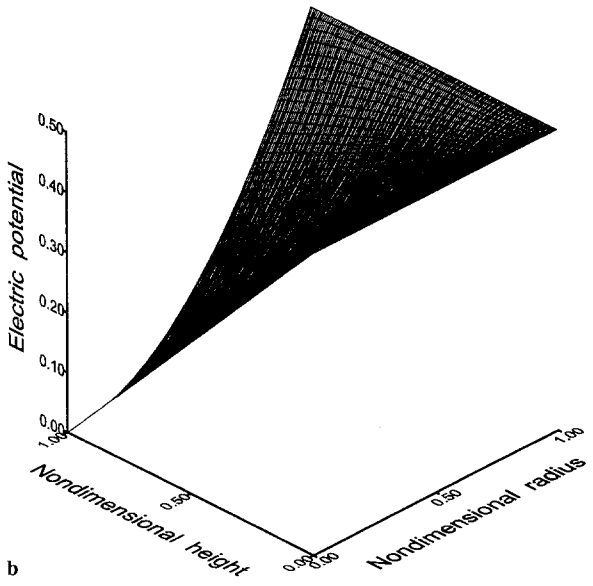

b

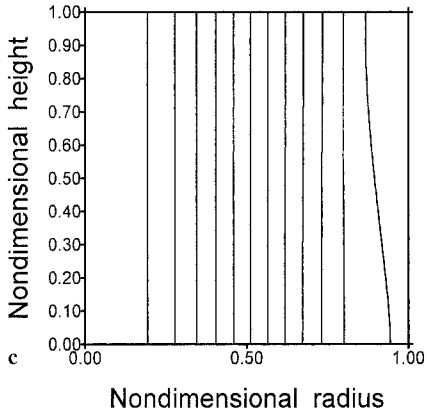

c

Fig. 11. Solution of the MHD problem for perfectly conducting walls ($H/R = 1$ and $\mathrm{Ha} = 100$). **a** Azimuthal velocity field, **b** Electric potential field, **c** Iso-lines of electric current

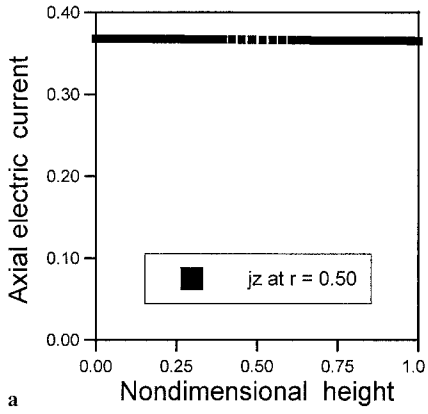

a

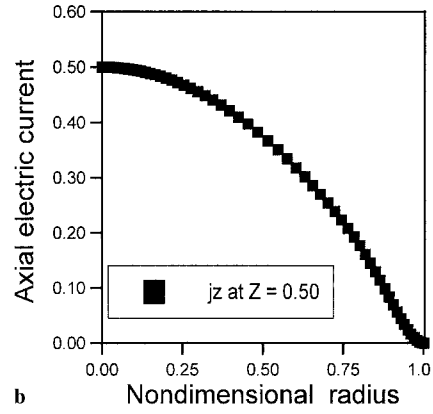

b

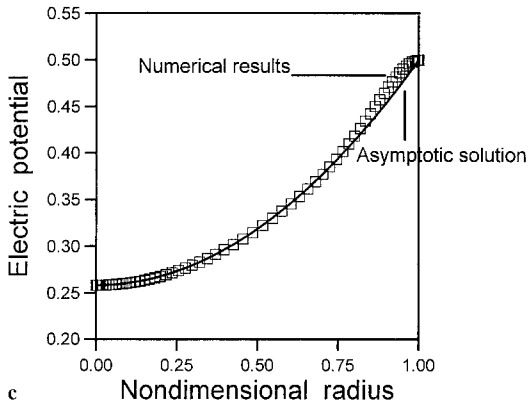

c

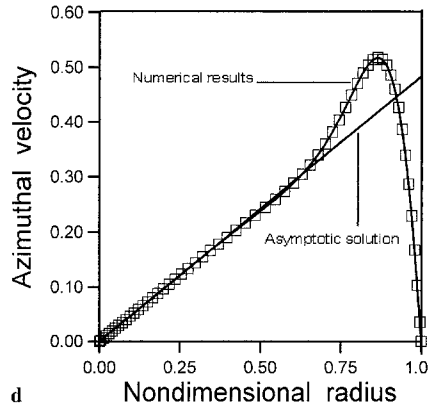

d

Fig. 12. Perfectly conducting walls. Electric current, potential and azimuthal velocity distributions for $H/R = 1$ and $\mathrm{Ha} = 100$. **a** Distribution of the axial electric current at $r = 0.50$, **b** Distribution of the axial electric current at $Z = 0.50$, **c** Distribution of the electric potential at $Z = 0.50$: comparison with asymptotic solution, **d** Distribution of the azimuthal velocity component at $Z = 0.50$: comparison with asymptotic solution

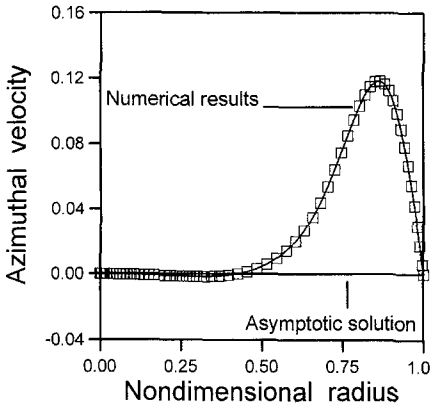

Fig. 13. Only the bottom of the cylinder is conducting. Electric potential and azimuthal velocity distribution in $Z = 0.50$

3.2.2 Electrically conducting walls

In this case, the two end walls and the vertical wall are infinitely conducting. The boundary conditions on φ are deduced from the cancelling of the tangential component of the electric current at the interface between the fluid and the walls. They are written:

$$\frac{\partial \varphi}{\partial r}(r=0)=0; \qquad \varphi(Z=1)=\frac{r^2}{2}; \qquad \varphi(r=1)=\varphi(Z=0)=\frac{1}{2}.$$

The cancelling of j_r near the walls prevents the existence of Hartmann layers. This explains the more monotonous structure of the velocity field which varies linearly as a function of r and Z through the whole fluid (Fig. 11 a).
The core solution

$$V_\theta = rZ,$$

$$\varphi = \frac{(r^2-1)\,Z+1}{2}$$

satisfies the azimuthal momentum equation and the boundary conditions. The value of the axial current in the core is now of $O(1)$ and can be easily obtained from this solution:

$$j_z = -\frac{\partial \varphi}{\partial Z} = \frac{1-r^2}{2}.$$

The numerical results in Fig. 12 are in excellent agreement with these estimations.

The situation can be interpreted as though the disk generates because of its rotation, in its inside, a radial gradient of the potential and communicates to the other two walls the value of φ felt at its end situated in $r = 1$. The bottom is therefore globally at a higher potential than the disk, which is at the origin of the electric current of order 1 which circulates from bottom to top. Figures 12 c and 12 d give the distributions of φ and V_θ along the $Z = 0.50$ line. As can be seen the computed values are in excellent agreement with the asymptotic solution.

3.2.3 Intermediate cases

Three different cases of combination of insulating and conducting walls are presented in Figs. 13–15. Figure 13 shows the case when all the walls are insulating except the bottom wall which is perfectly conducting. Here, the radial component of the electric current in $Z = 0$ is

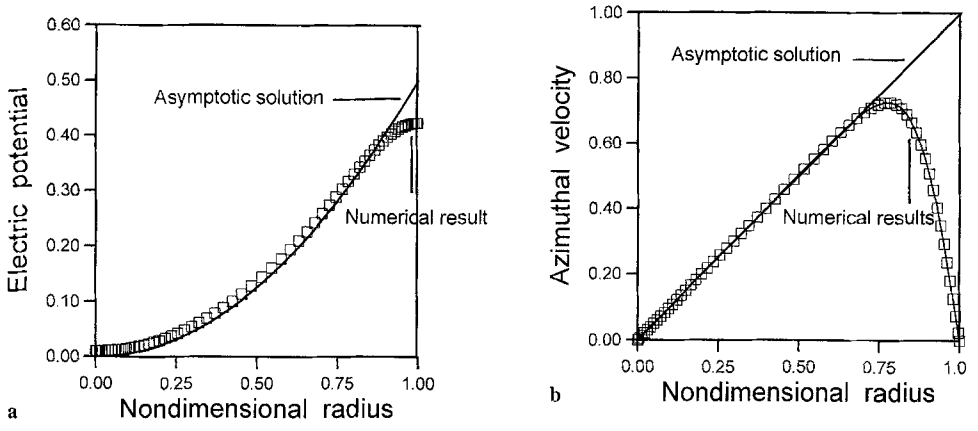

Fig. 14. Only the rotating disk is conducting. Azimuthal velocity distribution in $Z = 0.50$. **a** Electric potential, **b** Azimuthal velocity

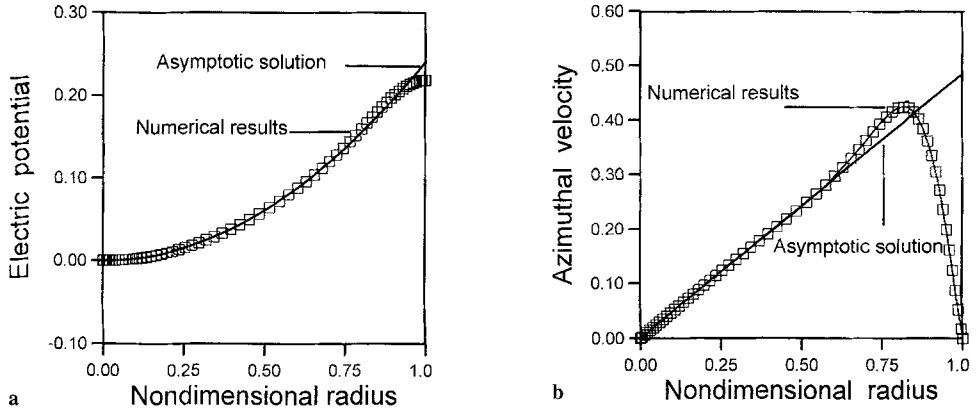

Fig. 15. Both the rotating disk and the bottom of the cylinder are conducting, the vertical wall is insulating: electric potential and azimuthal velocity distribution in $Z = 0.50$. **a** Electric potential, **b** Azimuthal velocity

zero and prevents once more the existence of a Hartmann layer on the bottom, which for this reason cannot be submitted to any velocity gradient and therefore imposes to the core to remain at rest ($V_\theta = 0$). The matching with the rotating disk occurs in the Hartmann layer in $Z = 1$.

For the case where only the disk is perfectly conducting the solution given in Fig. 14 shows a non-rotating core and a good agreement with the asymptotic solution. The results corresponding to an insulating vertical wall are presented in Figs. 15a and 15b and show a linear variation of the tangential velocity throughout most of the chamber. A perfect agreement with the asymptotic solution ($V_\theta = rZ$; $\varphi = (r^2/2)\, Z$) can be noticed in both figures.

4 Conclusion

A numerical procedure to predict the flow in a cylindrical cavity with a rotating end wall has been proposed. In a pure hydrodynamic situation, the results have been successfully compared to experimental data published in the literature. In the presence of a strong vertical

magnetic field, the computed flow solution, electric potential and current distribution have been compared to asymptotic solutions which can be obtained when inertial effects are neglected. Here also the agreement is good. Finally, the influence of the electrical conductivity of the walls has been considered. The results indicate that one can control the behavior of the primary flow through a good choice of the electric conductivities of the disk and cylinder walls. In view of further laboratory experiments aiming at investigating the effect of a strong magnetic field on chemical phenomena occurring at the interface between a solid wall and a liquid metal flow (Barbier et al. [13]) the simple geometry studied in this paper appears to be a convenient tool which offers the possibility to vary velocity gradients by modifying the wall conductivities.

References

[1] Granger, R. A.: Introduction to vortex dynamics. V. Kármán Institute Lecture Series 1986-08, Volume 1 (1986).
[2] Tsitverblit, N., Kit E.: Numerical study of axisymmetric vortex breakdown in an annulus. Acta Mech. **118,** 79–95 (1996).
[3] Schultz-Grunow, F.: Der Reibungswiderstand rotierender Scheiben in Gehäusen. ZAMM **15,** 191–204 (1935).
[4] Daily, J. W., Nece, R. E.: Chamber dimension effects on induced flow and frictional resistance of enclosed rotating disks. J. Basic Eng. **82,** 217–231 (1960).
[5] Grohne, D.: Über die laminare Strömung in einer kreiszylindrischen Dose mit rotierendem Deckel. Nachr. Akad. Wiss. Göttingen Math.-Phys. Klasse **12,** 263–282 (1955).
[6] Thomlan, P. F., Hudson, J. L.: Flow near an enclosed rotating disk: analysis. Chem. Eng. Sci. **26,** 1591–1600 (1971).
[7] Bertela, M., Gori, F.: Laminar flow in a cylindrical container with a rotating cover. J. Fluids Eng. **104,** 31–39 (1982).
[8] Lang, E., Sridhar, K., Wilson, N. W.: Computational study of disk driven rotating flow in a cylindrical enclosure. J. Fluids Eng. **116,** 815–820 (1994).
[9] Alonso, C. V.: Steady laminar flow in a stationary tank with a spinning bottom. J. Appl. Mech. **42,** 771–776 (1975).
[10] Escudier, M. P.: Observations of the flow produced in a cylindrical container by a rotating endwall. Exp. Fluids **2,** 189–196 (1984).
[11] Ronnenberg, B.: Ein selbstjustierendes 3-Komponenten-Laser Doppler-Anemometer nach dem Vergleichsstrahlverfahren, angewandt für Untersuchungen in einer stationärem zylindersymmetrischen Drehströmung mit einer Rückströmblase. Max-Planck-Institut für Strömungsforschung, Bericht 20/1977.
[12] Hjellming, L., Walker, J.: Melt motion in a Czochalski crystal puller with an axial magnetic field: isothermal motion. J. Fluid Mech. **164,** 237–273 (1986).
[13] Barbier, F., Alemany A.: On the influence of a high magnetic field on the corrosion and deposition processes in the liquid Pb-17Li alloy. Fusion Eng. Des. Rev. **62,** 120–135 (1998).
[14] Patankar, S. V.: Numerical heat transfer and fluid flow. New-York: McGraw-Hill 1980.
[15] Michelsen, J. A.: Modeling of laminar incompressible rotating fluid flow, AFM 86-05, Ph. D. Dissertation, Dept. of Fluid Mechanics, Tech. Univ. of Denmark, 1986.

Authors' addresses: R. Bessaih and M. Kadja, Inst. de Génie Mécanique, Univ. de Constantine, Route d'Ain El. Bey, Constantine 25000, Algeria and Ph. Marty, Lab des Ecoulements Géophysiques et Industriels, B.P. 53 X, 38041 – Grenoble Cedex, France